Polymer Dynamics in Epoxy/Alumina Nanocomposites Studied by Various Techniques

Apostolos Kyritsis,[1] Georgios Vikelis,[1] Panayiotis Maroulas,[1] Polycarpos Pissis,[1] Boryana Milosheva,[2] Rumiana Kotsilkova,[2] Antonia Toplijska,[2] Clara Silvestre,[3] Donatella Duraccio[3]

[1]*Department of Physics, National Technical University of Athens, Zografou Campus, 15780 Athens, Greece*
[2]*Central Laboratory of Physico-Chemical Mechanics, Bulgarian Academy of Sciences, Academician G. Bonchev Street, Block 1, BG 1113 Sofia, Bulgaria*
[3]*Institute of Chemistry and Technology of Polymers, CNR, Via Campi Flegrei, 34, 80078 Pozzuoli NA, Italy*

Received 20 October 2010; accepted 12 January 2011
DOI 10.1002/app.34161
Published online 12 April 2011 in Wiley Online Library (wileyonlinelibrary.com).

ABSTRACT: Epoxy/alumina nanocomposites of various compositions were prepared by dispersing modified and nonmodified boehmite nanoparticles in diglycidyl ether of bisphenol-A using diethylenetriamine as curing agent. Measurements of the viscosity of the nanodispersions provided information on particle–particle and particle–resin interactions. The structure of the nanocomposites was studied by scanning electron microscopy on fractured samples. Effects of nanoparticles on polymer dynamics was studied in detail by dynamic mechanical thermal analysis and two dielectric techniques, broadband dielectric relaxation spectroscopy and thermally stimulated depolarization currents. Three secondary relaxations, γ, β, and ω, the segmental α relaxation associated with the glass transition, and an interfacial relaxation, in the order of increasing frequency/decreasing temperature, were observed and studied. A correlation between viscosity (of the nanodispersions), storage modulus, glass transition temperature, real part of dielectric permittivity, and ductility of the nanocomposites was observed. © 2011 Wiley Periodicals, Inc. J Appl Polym Sci 121: 3613–3627, 2011

Key words: epoxy/alumina nanocomposites; boehmite; polymer dynamics; glass transition; dielectric properties

INTRODUCTION

Organic–inorganic polymer nanocomposites (Ncs) have attracted much interest in recent years, as they may exhibit significant improvement of various properties of the polymer matrix, in particular mechanical properties, thermal stability, and barrier properties, at much lower filler fractions than conventional composites (macrocomposites).[1–3] Polymer dynamics studies in such systems, in particular studies of segmental dynamics and the related glass transition, are of fundamental interest for understanding, and thus tailoring, properties improvement at the molecular level.[4,5] We may expect that chain dynamics in the Ncs is modified, as compared with the neat polymer, due to interactions at the polymer–filler interfaces. In fact, computer simulations and experiments with model systems provide evidence that polymeric chains in the vicinity of a solid surface, within a distance of a few nm, exhibit different organization (density, chain configuration) and properties (thermal transitions, molecular mobility), as compared with chains in the bulk.[6] Molecular dynamics simulations show that relaxation times may increase or decrease, as compared with the bulk material, depending on the type and strength of interaction and the roughness of the surface.[7] Also, the results of experiments with model systems, in particular glass forming liquids and polymers confined in porous glasses and thin polymer films, are often discussed in terms of a layer of molecules with modified dynamics at the interface with the solid surface.[8]

Results reported in literature on chain dynamics in real polymer Ncs, on the other hand, in particular on segmental dynamics associated with the glass transition, often appear controversial and confusing, as dynamics (often quantified in terms of glass transition temperature) may become faster or slower or show no change, it may be homogeneous or heterogeneous etc.[9] Obviously, several factors, next to polymer–filler interactions, such as filler size, roughness and morphology (degree of dispersion), may affect polymer dynamics in Ncs and should be

Correspondence to: A. Kyritsis (akyrits@central.ntua.gr).
Contract grant sponsor: European Community's Seventh Framework Programme; contract grant number: FP7/2007-2013 under grant agreement n° 218331 NaPolyNet (www.napolynet.eu).
Contract grant sponsor: NSF-BG project DO-02-53 (2009–10) and the CNR-BAS (2010–12) bilateral project.

critically considered. Also, results obtained by various experimental techniques should be critically compared with each other, as each technique probes molecular mobility in a different way.[10] It has been pointed out that two main contradictory effects of nanoparticles on chain dynamics should be properly considered[11,12]: dynamics may become slower, in particular close to interfaces, due to constraints imposed to the motion of the chains by the rigid nanoparticles, this effect being more pronounced in the case of covalent bonds between the two components (hybrid organic–inorganic Ncs); at the same time, dynamics may become faster as a result of increase of free volume due to loosened molecular packing of the chains (plasticization).

In this article, we report on polymer dynamics in epoxy/alumina Ncs. Because of the wide range of potential applications, epoxies are being widely used as polymer matrices in Ncs. Results obtained with epoxy/layered silicate (clay) Ncs have been reviewed by Becker and Simon.[13] Both a constant or increased glass transition temperature T_g and a reduction of T_g with increasing organically modified clay addition have been reported. Sun et al.[14] studied several epoxy Ncs with various inclusions (silica, silver, aluminum, carbon black) and observed a depression of T_g, related with enhanced polymer dynamics due to extra free volume at the resin–filler interface. Miyagawa et al.[15] observed a slight increase of T_g in epoxy/clay Ncs (by 1.5°C at 6 vol %). Lu and Nutt[16] investigated the relaxation behavior of epoxy/clay Ncs by a combination of standard and temperature modulated differential scanning calorimetry (DSC). Addition of the intercalated nanoparticles resulted in a slower overall relaxation, a wider distribution of relaxation times and higher T_gs. A domain relaxation model was proposed that included three possible relaxation modes.[16] Measurements by various techniques in epoxy/carbon particles Ncs showed an increase of T_g as compared with the neat polymer matrix. In agreement with that the time scale of the segmental relaxation associated with the glass transition increased in the Ncs, whereas that of the secondary β relaxation remained unaffected.[17] Dielectric and DSC measurements in rubbery epoxy networks modified with polyhedral oligomeric silsesquioxanes (POSS) nanoparticles covalently bound to the chains as dangling blocks showed that a fraction of polymer is immobilized making no contribution to the glass transition, whereas the rest exhibits a slightly faster segmental dynamics due to increased free volume resulting from loosened molecular packing of the chains (plasticization by the bulky POSS units).[5]

Similar to other oxides, alumina has been used by several investigators as inclusion in polymer Ncs, although by far less frequently than silica, and effects on polymer dynamics and glass transition have been studied in some cases. In a series of articles, Ash et al.[18,19] investigated poly(methyl methacrylate) (PMMA)/alumina Ncs and observed that already at low filler content, below 1 wt %, T_g drops by about 25°C when compared with the neat polymer and shows no more changes on further additions of filler. No significant T_g changes, with respect to the neat polymer, were observed in Ncs prepared with chemically treated with silane coupling agent alumina nanoparticles and in macrocomposites. Poor adhesion between filler and polymer was made responsible for the drop of T_g, which was further rationalized in terms of a percolation model proposed for the T_g reduction in thin polymer films.[20] A different interpretation in terms of internal stresses at the polymer–particle interface and heterogeneous dynamics was proposed by Narayanan et al.[21] for similar results obtained with PMMA/alumina Ncs on the basis of multispeckle X-ray photon correlation spectroscopy. Interestingly, heating to 220°C followed by slow cooling caused the T_g to increase to a value close to that for neat PMMA, in analogy to the chemically treated samples in Refs. 18 and 19. In another work, dielectric and DSC measurements showed a slight reduction of T_g and of its activation energy in epoxy/alumina nanowires Ncs, as compared with the neat polymer, which was rationalized in terms of a proposed coarse-grained confined-region structure model.[22] A suppression of T_g was observed also in semicrystalline poly(ethylene terephthalate)/alumina Ncs and interpreted in terms of increased mobility near the surface of the filler, whereas the degree of crystallinity remained practically unaffected.[23] In another semicrystalline thermoplastic, poly(ether-ether-ketone), the presence of alumina, as well as of silica, with a uniform distribution of the nanoparticles, resulted in an increase of the degree of crystallinity and of thermal stability.[24]

In contrast to the results reported above, DSC and dynamic mechanical thermal analysis (DMTA) measurements in epoxy/alumina Ncs by Vassileva and Friedrich[25] revealed an increase of T_g, which was highest for alumina nanoparticles chemically treated by reactive silane coupling agent. Also, the β relaxation became slower in the Ncs with a concomitant increase of its activation energy and a suppression of the short-range cooperative motions related to the high-temperature part of the relaxation. DMTA measurements in polyurethane latex/water dispersible boehmite alumina Ncs revealed also a slight increase of T_g, whereas no effect was observed by dielectric relaxation spectroscopy (DRS) on the segmental α relaxation associated with the glass transition.[26] Finally, fluorescence measurements in polymer/alumina Ncs prepared by spin coating films

from solutions showed a substantial increase of T_g in poly(2-vinyl pyridine) (P2VP) Ncs, a moderate decrease in PMMA Ncs, and practically no change in polystyrene (PS) Ncs, always with respect to the neat polymer.[27] By analogy with thin polymer films, these results were explained by wetted P2VP-nanofiller interfaces with attractive interactions, nonwetted PMMA-nanofiller interfaces (free space at the interface), and wetted PS-nanofiller interfaces lacking attractive interactions, respectively. The presence of wetted or nonwetted interfaces was controlled by choice of solvent.[27]

We like to draw attention to the fact that interpretation of experimental results on polymer dynamics may become more complex in thermoset Ncs, including epoxy network Ncs, as compared with Ncs based on thermoplastic matrices. The reason for this is that curing reactions and cross-linking density may be modified by the presence of the nanofillers or the matrix may be plasticized by smaller molecules present in the network.[13] This "secondary" effect (which is present also in thermoplastic Ncs prepared by polymerization in the presence of the nanoparticles[18,19]) should be distinguished from the "primary" one of direct influence of the nanofillers on chain dynamics.

The epoxy/alumina Ncs under investigation in this work were prepared by *in situ* polymerization of epoxy resin oligomer (DER 332) in the presence of alumina nanoparticles (boehmite, SASOL, Germany) using an amine type hardener. Three types of alumina have been used: Disperal D40 (nonmodified boehmite, crystallite size 40 nm); Disperal OS1 and Disperal OS2, treated by the producer with different type modifiers, more details being given in the next section. The fraction of the filler was varied between 0 and 5 mass %. Measurements of the viscosity of the nanodispersions provided information on particle–particle and particle–resin interactions. The structure of the Ncs was studied by scanning electron microscopy (SEM). Polymer dynamics, in particular glass transition, and mechanical properties were studied by DMTA (1–100 Hz, −100 to 180°C). For a more detailed study of polymer dynamics two dielectric techniques were employed, namely broadband DRS (10^{-1}–10^{6} Hz, −150 to 120°C) and thermally stimulated depolarization currents (TSDC; −150 to 80°C). The broad frequency and temperature ranges of DRS allow us to follow local (secondary) and cooperative relaxations, as well as electrical conductivity,[28] whereas the use of TSDC enables to extend the frequency range of measurements down to 10^{-2}–10^{-4} Hz,[29] *i.e.*, a frequency range not easily accessible by DRS measurements in the frequency domain. Results on polymer dynamics obtained by the various techniques employed (DMTA, DRS, TSDC) are critically compared with each other, correlated to those of viscosity and SEM measurements on the same samples, and discussed in relation to previous work mentioned above.

It should be noted that in recent years electrical and dielectric measurements were employed to study epoxy/alumina nanocomposites, for a different reason, however, than in this article, namely in relation to their potential application as insulating materials.[30–33] Next to mechanical and thermal properties (glass transition), specific properties significant for that application, such as permittivity, loss tangent, space charge accumulation, breakdown strength, tree formation, and partial discharge resistance, were studied. The results suggest that the overall performance is improved on addition of the nanofiller. The extent of modification of the various properties depends on the amount of filler, the degree of dispersion and specific interfacial interactions.

EXPERIMENTAL

Materials

Epoxy/alumina Ncs were prepared using low viscosity diglycidyl ether of bisphenol-A (DGEBA, commercial name DER 332, Sigma Aldrich) as epoxy resin oligomer, diethylenetriamine (Fluka) as hardener, and boehmite alumina nanoparticles (AlO(OH)) provided by Sasol (Germany) as filler. Three types of boehmite alumina with primary crystallite size 40 nm were used, one unmodified and two modified, their characteristics being listed in Table I. The content of boehmite alumina was varied as 1, 3, and 5 mass %. These systems are amenable to preparing nanocomposites by direct cross-linking polymerization technique, where the nanofillers are subject to dispersion in the liquid medium and the mixture is subsequently polymerized to form the nanocomposite. However, the nanoparticles as received are highly agglomerated (Table I), hence these agglomerates have to be broken down to

TABLE I
Characteristics of the Boehmite Alumina Particles Used

	Disperal® D40	Disperal® OS1	Disperal® OS2
Density (g/ml)	2.9	2.7	2.7
Surface area (m^2/g)	105	265	272
Particle size (μm)	50	45	45
Modifier	No modifier	p-Toluenesulfonic acid $SO_3H(C_6H_4)CH_3$	Alkyl (C10–C13) benzenesulfonic acid $SO_3H(C_6H_4)(CH)_n CH_3$

individual nanoparticles, *e.g.*, by sonication approach. Consequently, the polymer dispersions were prepared by a two-step direct mixing method. The dispersions were first mixed mechanically for 30 min at ambient temperature for initial wetting of the fillers. Then an ultrasonic bath was used for 30 min at a temperature of 40°C for further dispersion of the boehmite alumina nanofiller in the resin. Different samples were prepared and cured at ambient conditions and postcured in the course of 2 h at 100°C for structure and properties stabilization.

Samples are typically characterized by the type of particle modification used and the composition, *e.g.*, DER/OS2(97/3) for a sample with 3 mass % of Disperal OS2 particles (Table I).

Methods

The rheological parameters of the fluid compositions were determined using Rheotron Brabender rotational viscometer (cone-plate geometry) under a steady state and oscillatory flow regime within the shear rate range 0.3–100 s^{-1}.

SEM micrographs were taken with a Philips 501 microscopy. Micrographs of fracture surfaces of the neat resin and compositions with 5 mass % of boehmite alumina D40, OS1, and OS2 were taken. The specimens were coated with gold before observation to avoid charge build up.

DMTA tests (DMTA III, Polymer Laboratories) were conducted to study the thermomechanical properties of the nanocomposites under dynamic loading conditions and to determine glass transition temperatures. The dual cantilever mode was used with fixed oscillation amplitude of 10 μm and frequencies 1, 10, and 100 Hz. The temperature range varied from −100 to 180°C, applying a heating step of 3°C/min. All the DMTA specimens were rectangular bars with dimensions of 3 mm × 6 mm × 20 mm.

For DRS measurements[28] the complex dielectric constant (dielectric permittivity, dielectric function), $\varepsilon^*(f) = \varepsilon'(f) - i\varepsilon''(f)$, was determined as a function of frequency, f, (10^{-1}–10^6 Hz) at constant temperature (−150 to 120°C, controlled to better than ±0.1K), using a Novocontrol Alpha Analyzer in combination with a Novocontrol Quatro Cryosystem. The samples were circular films of typically 20-mm diameter and about 1-mm thickness and were placed between brass electrodes.

TSDC is a dielectric technique in the temperature domain and consists of measuring the thermally activated release of stored dielectric polarization.[29] By this technique the sample is inserted between the plates of a capacitor and polarized by the application of an electric field E_p at temperature T_p for time t_p, which is large compared with the relaxation time of the dielectric relaxation under investigation. With the electric field still applied, the sample is cooled to a temperature T_0, which is sufficiently low to prevent depolarization by thermal energy, and then is short-circuited and reheated at a constant rate b. The discharge current generated during heating is measured as a function of temperature with a sensitive electrometer. TSDC corresponds to measuring dielectric loss at a constant low frequency in the range 10^{-4}–10^{-2} Hz. It is characterized by high sensitivity and high resolving power.[29] TSDC measurements were carried out using a Keithley 617 electrometer in combination with a Novocontrol sample cell for TSDC measurements. Typical experimental conditions were 50°C for T_p, 2 kV/cm for E_p, 5 min for t_p, 10°C/min for the cooling rate to $T_0 = -150$°C, and 3°C/min for the heating rate b. Samples and electrodes were similar to those used for DRS measurements.

RESULTS AND DISCUSSION

Viscosity measurements

Results of viscosity measurements for the various fluid compositions at room temperature are shown in Figure 1. For each type of filler, viscosity increases with increasing filler content due to the increased number of contacted solid particles in the low viscosity liquid matrix. At each composition (mass fraction of filler) viscosity increases in the order OS1, OS2, D40. These results suggest that dispersions containing nonmodified D40 demonstrate strong particle–particle interactions. Treating the boehmite particles with the modifiers decreases the particle–particle interactions and increases the affinity

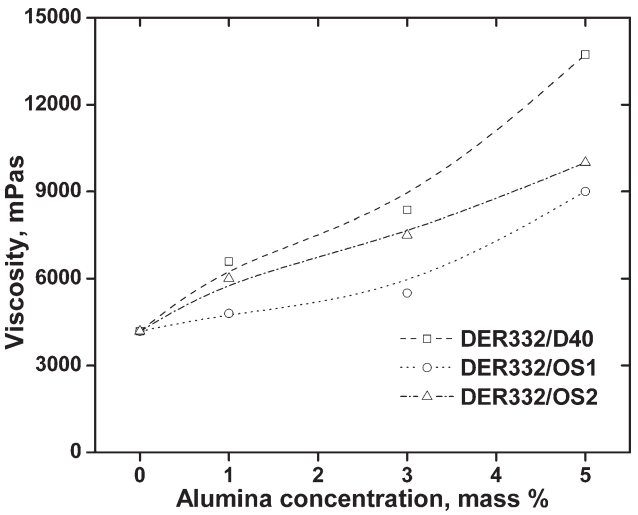

Figure 1 Viscosity of nanodispersions against nanofiller concentration at room temperature for various Ncs indicated on the plot.

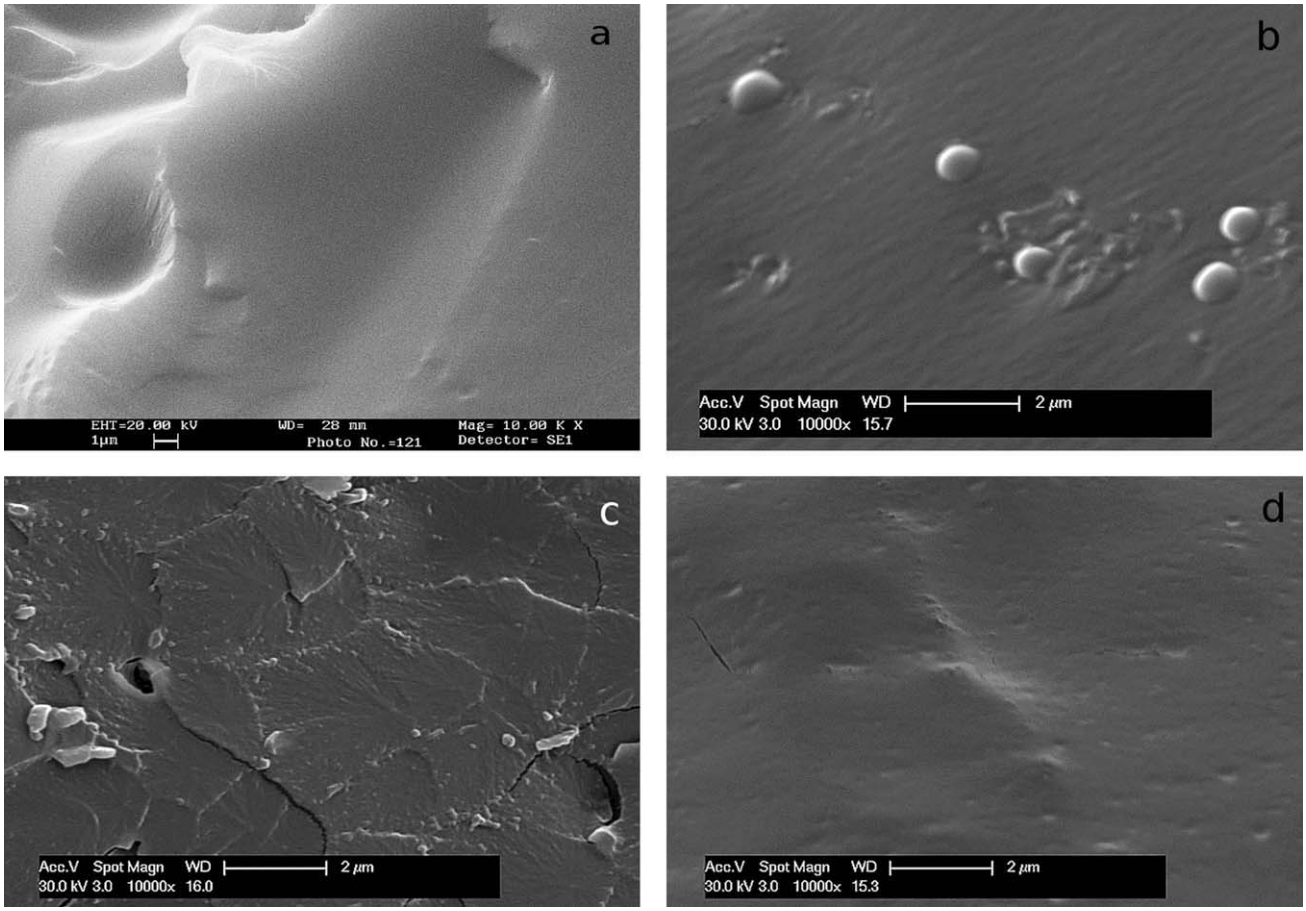

Figure 2 Morphology of neat epoxy resin (a) and epoxy/alumina nanocomposites DER/D40 (95/5) (b), DER/OS1 (95/5) (c), and DER/OS2 (95/5) (d).

between the nanofiller and the resin, the strongest effect being demonstrated for OS1. Thus, the degree of dispersion of boehmite particles in the epoxy matrix increases in the order D40, OS2, OS1, where the OS1 treated boehmite particles demonstrate much better dispersion compared with the untreated one D40.

Interestingly, Karger-Kocsis and coworkers reported that boehmite alumina nanoscale dispersed in both low and high density polyethylene had practically no effect on melt rheology (175°C), this result being of significant interest with respect to processing of thermoplastic nanocomposites.[34]

Fracture behavior and morphological characterization (SEM)

The SEM micrograph of fractured surface of the neat epoxy system indicates glassy and homogeneous microstructure as shown in Figure 2(a). This supports brittle nature and poor impact strength of the epoxy resin. The SEM micrographs of fractured surfaces of Ncs modified with 5 mass % of boehmite alumina D40, OS1, and OS2 [Figs. 2(b–d), respectively], reveal significant differences in the morphology of the Ncs with unmodified and modified nanoparticles. While on the fractured surface of the sample DER/D40 (95/5) large number of small agglomerates could be observed, the fractured surface of the sample DER/OS1 (95/5) is rather rough, which indicates that the crack propagation is difficult, and shows relatively homogeneous structure with few aggregates embedded in the matrix. The image of fractured surface of the DER/OS2 (95/5) sample presents smooth and homogeneous structure without discernible particles or agglomerates.

DMTA measurements

Figure 3 shows results of DMTA measurements: storage modulus E' and tan δ of neat epoxy resin and the Ncs at a fixed filler fraction of 1 mass % against temperature at 1 Hz. In Figure 3(a), an overall decrease of E' of epoxy resin is observed by addition of the nanofiller, both below and above T_g. The reduction of the E' values in the solid-state region increases in the order D40, OS2, OS1. This indicates that the stiffness of the Ncs is decreased but the toughness is increased as compared with the neat epoxy matrix. Muehlhaupt and coworkers[35] reported

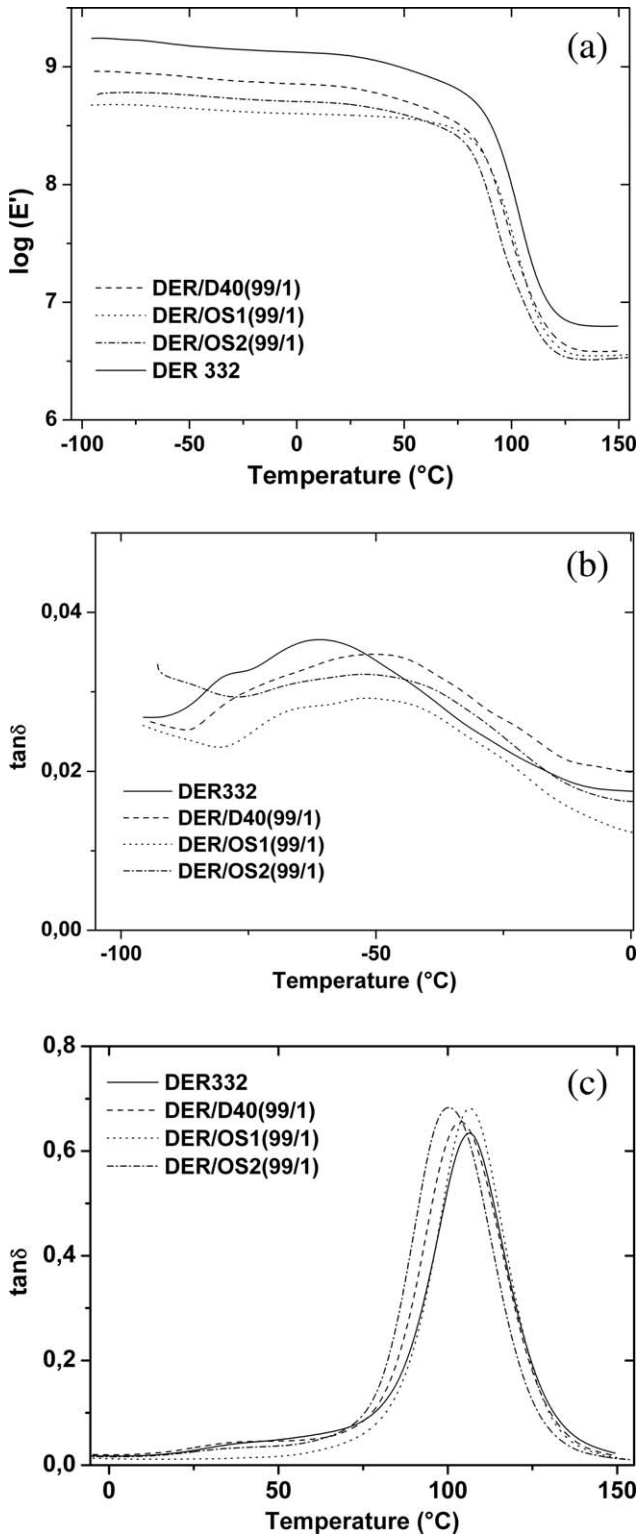

Figure 3 Storage modulus E' (a) and tan δ (b, c) of neat epoxy resin and the Ncs against temperature at 1 Hz.

that the type of organic modification of boehmite has a significant effect on the mechanical properties of isotactic polypropylene/alumina nanocomposites. Brostow et al.[36] reported that increase of filler–matrix interfacial adhesion in low density polyethylene/boehmite composites, arising from the use of silane coupling agent, gave rise to significant improvement of tribological properties.

Interestingly, viscosity of the nanodispersions in Figure 1 decreases in the same order as E' in Figure 3. Correlation of the E' results with those of the real part of dielectric permittivity ε', to be discussed later, suggests that the drop of E' in the Ncs is related to an increase of molecular mobility, probably at the polymer–filler interface.[23] This conclusion is supported by the results by Ash et al.[18,19] in PMMA/alumina Ncs, where a decrease of both E' and of T_g and a room-temperature brittle-to-ductile transition were observed, and by Vassileva and Friedrich in epoxy/alumina Ncs[25] where an increase of both E' and of T_g was observed.

Three peaks are observed in the temperature dependence of loss tangent in Figures 3(b) and 3(c). The most pronounced one at about 100°C [Fig. 3(c)], accompanied by a significant drop of E' in the same temperature region, corresponds to the glass transition and its peak temperature, listed in Table II together with the corresponding loss tangent value, is a good measure of T_g (as confirmed also by DSC measurements not shown here). Thus, T_g decreases in the Ncs with D40 and OS2 fillers, as compared with the neat epoxy matrix, and increases again to the neat epoxy value in the Nc with OS1 filler. At the same time the loss peak height increases in the Ncs. This increase may be related to the toughness improvement in the Ncs. The drop of T_g in the Ncs is in agreement with results obtained in several polymer/alumina Ncs,[18,19,23] whereas its increase back to the neat polymer value for the chemically treated (OS1) filler resembles the results in Refs. 18 and 19.

A loss peak is observed in the glassy state at about −50°C [Fig. 3(b)], which, in agreement with the literature,[13,17,22,25] is attributed to the β relaxation. Peak temperature and loss tangent peak value are also listed in Table II. The most pronounced effect of the addition of filler is a significant shift of the peak temperature to higher temperatures, suggesting an antiplasticization effect of the fillers,[25]

TABLE II
DMTA Results for the Peak Temperature and the Loss Tangent Peak Height of the α and the β Relaxations in the Ncs at 1% Mass Filler

Sample	Peak temperature T_α (°C)	α Loss peak height	Peak temperature T_β (°C)	β Loss peak height
Neat epoxy	107	0.66	−64	0.037
DER/D40	102	0.67	−48	0.035
DER/OS1	108	0.70	−53	0.029
DER/OS2	101	0.70	−54	0.032

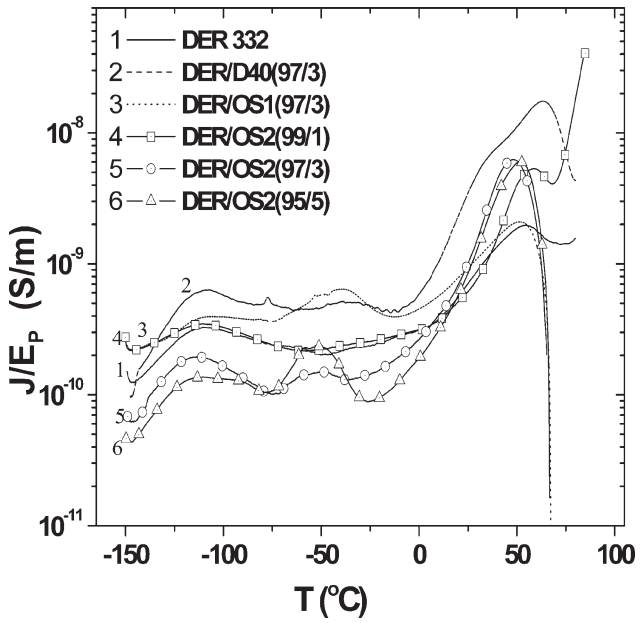

Figure 4 TSDC thermograms for several compositions indicated on the plot. The polarization temperature T_P was 53°C.

more pronounced for the unmodified filler. The β relaxation is also dielectrically active and will be studied extensively by dielectric techniques in the following sections, where also the DMTA results will be discussed in more detail.

We will comment on the third peak in Figure 3(c), at about 30°C, later in relation to DRS measurements.

TSDC measurements

Figure 4 shows TSDC thermograms in the temperature range from −150 to 80°C for several compositions: the neat epoxy matrix, three Ncs with different type of filler (D40, OS1, OS2) at the same mass fraction of 3%, and three Ncs with the same type (OS2) and different mass fraction of filler (1, 3, and 5%). These compositions were selected for a detailed study of effects of type and of amount of filler on polymer dynamics by dielectric TSDC and DRS techniques. The depolarization current density J has been normalized to the same polarizing field E_P (different thicknesses of the samples), so that TSDC peaks for different samples can be compared with each other not only with respect to temperature position but also to magnitude. The former provides information on time scale and the latter on concentration of dipoles (relaxing units in general) giving rise to the corresponding relaxation.[29]

Three dispersion regions (single or multiple peaks) are discerned in Figure 4. In agreement with TSDC results obtained with various epoxy systems in the past,[17,37,38] the first two peaks, in the order of increasing temperature, at subzero temperatures, are designated as β and ω relaxation, respectively. The β relaxation has been assigned to dipolar rotation of the pendant hydroxyl group generated on the ring opening of the epoxy group; presumably it undergoes a crankshaft motion which involves the glycidyl portion of the resin structure.[39,40] A detailed study by using the peak resolving thermal sampling mode of TSDC[38] has indicated that the β relaxation is double, which was interpreted in terms of the lower temperature (faster) part arising from dipolar motions in the less-dense regions of the network and the higher temperature (slower) part from dipolar motions in the more-dense regions of the network. In another work, DMTA and NMR measurements in a dense amino-cured epoxy network revealed also the double nature of the (mechanical) β relaxation, with the two parts being attributed to local motions at the spatial scale of one epoxy-amine repeat unit (lower temperature part) and to cooperative motions involving at least six units (higher temperature part).[41] The less frequently studied ω relaxation has been attributed to motions of phenyl rings in the looser part of the network.[38] Both β and ω relaxations in Figure 4 are affected by the presence of the filler. We will discuss these effects in the next section in relation to DRS measurements.

The depolarization current density in Figure 4 increases significantly at temperatures higher than about 0°C, indicating significant contribution of conductivity and space charge polarization. TSDC experiments with polarization temperature T_P close or above T_g determined by DMTA (Fig. 3 and Table II), as usually done[29,37,38] for following the α relaxation associated with the glass transition (dynamic glass transition), failed to provide information on the α relaxation, as this was masked by the significant increase of conductivity, similar to previous work.[17,37,38] For that reason, after several preliminary experiments, T_P in Figure 4 was chosen much lower than T_g, around 50°C, in an attempt to study the interfacial Maxwell-Wagner-Sillars (MWS) relaxation. The latter arises from accumulation of charges at the interfaces between regions of different conductivity and dielectric constant and, thus, its study provides information on morphology.[5,10,29] Please note that the MWS peak is present also in the neat epoxy sample, suggesting that also this sample is heterogeneous, in consistency with the results for the β relaxation discussed in the previous paragraph. Conductivity and MWS relaxation will be discussed in more detail in the next section in relation to DRS measurements.

DRS measurements

Compared with TSDC, DRS measurements provide the possibility to vary both frequency and temperature

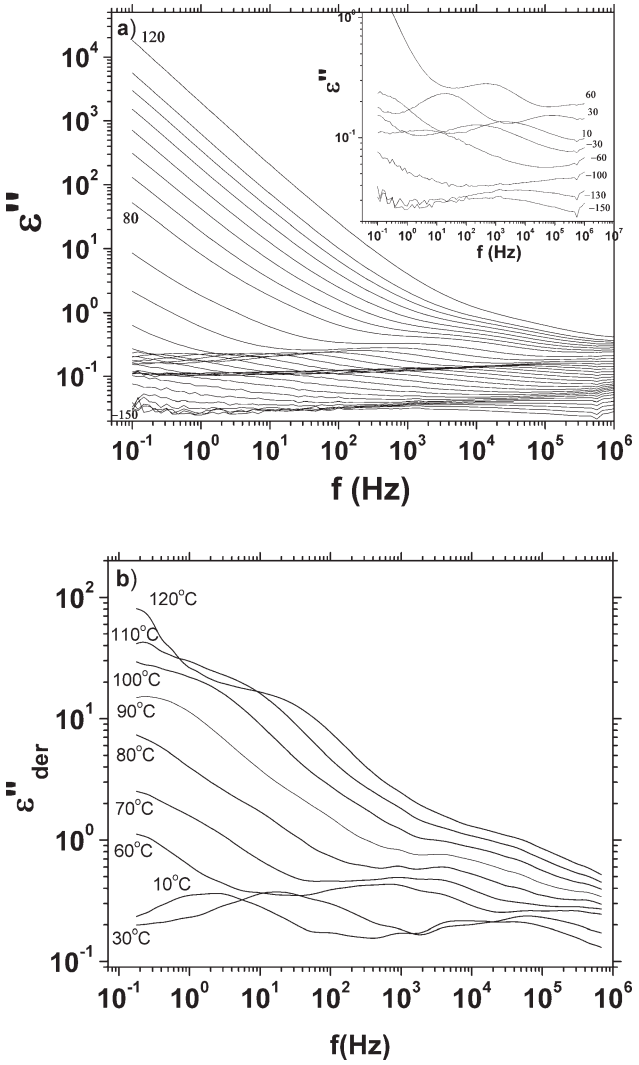

Figure 5 (a) Dielectric loss ε″ against frequency f at several temperatures for the sample DER/OS2 (95/5). The inset shows ε″(*f*) at selected temperatures indicated on the plot. b) ε''_{der} (*f*) plots obtained by employing the ε′-derivative representation for the same sample at several high temperatures indicated in the plot.

in wide ranges (10^{-1}–10^6 Hz and −150 to 120°C, respectively, in this study) and thus to study relaxations in more detail. As a typical example of measurements, Figure 5a shows for the sample DER/OS2 (95/5) log–log plots of the imaginary part of dielectric permittivity (dielectric loss) ε″ against frequency f at several temperatures in steps of 10°C at lower temperatures and of 5°C at higher temperatures. The inset shows ε″ (*f*) plots at selected temperatures, where we can follow three relaxations; the β and ω relaxations studied also by TSDC (Fig. 4) and, at lower temperatures, a faster γ relaxation. The latter could not be followed by TSDC, as it is out of the temperature range of measurements at the equivalent frequency of TSDC measurements of 10^{-4}–10^{-2} Hz.[29] At higher temperatures, on the other hand, in particular higher than T_g of about 100°C (Table II), and low frequencies, where the α relaxation associated with the glass transition (dynamic glass transition) should enter into our frequency window from the low-frequency side, the behavior is dominated by high values of ε″ arising from dc conductivity, as indicated by the approximately linear increase of losses with decreasing frequency.[5,28] To observe the relaxation peaks masked by the conductivity we employed, alternatively, the ε′-derivative representation,[42] $\varepsilon''(f) \approx \varepsilon''_{der}(f) = -(\pi/2)\partial\varepsilon'/\partial \ln(2\pi f)$, which is free from the dc conductivity (but not from conductivity related polarization effects). In Figure 5(b) we present ε''_{der} (*f*) plots for the sample DER/OS2 (95/5) at several high temperatures indicated on the plot. We observe that the relaxation peak related to ω relaxation process is clearly visible in the plots recorded at low temperatures while at higher temperatures the α relaxation peak is discerned (clearly separated at 120°C). The plots indicate, however, that conduction polarization effects take place at relatively high temperatures (close to T_g) resulting in a poor separation of segmental α relaxation peak from other low frequency dispersions even in the ε′-derivative representation. Therefore, a more detailed analysis within the frame of this data representation is required for any quantitative investigation of the underlying molecular processes. It would be interesting to further follow this point in future work.

Measurements similar to those shown in Figure 5 (also for the real part of dielectric permittivity ε′, where relaxations give rise to steps (drops)) were obtained for all six compositions of Figure 4, where polymer dynamics was studied by dielectric techniques. In the following the results for the various relaxations will be shown in comparative plots based on the raw data, before we proceed in the next section with analysis by fitting model functions to the experimental data. To get an overall overview of the various relaxations we show in Figure 6 the comparative isochronal (constant frequency) plot of ε″ against temperature T for all the compositions studied. The data have been recorded isothermally (Fig. 5) and have been here re-plotted. Because of the small temperature step of isothermal measurements, the results are shown in the form of lines connecting the experimental points rather than individual points. A low constant frequency of 1 Hz has been chosen for the plots in Figure 6 to take advantage of the higher peak resolving power of DRS measurements at lower frequencies and to facilitate comparison with the TSDC plots in Figure 4 (and the DMTA plots in Fig. 3). Because of the low frequency, the γ relaxation is out of the temperature range of presentation [compare the inset to Fig. 5(a)] and only the β and ω relaxations are observed. The two relaxations

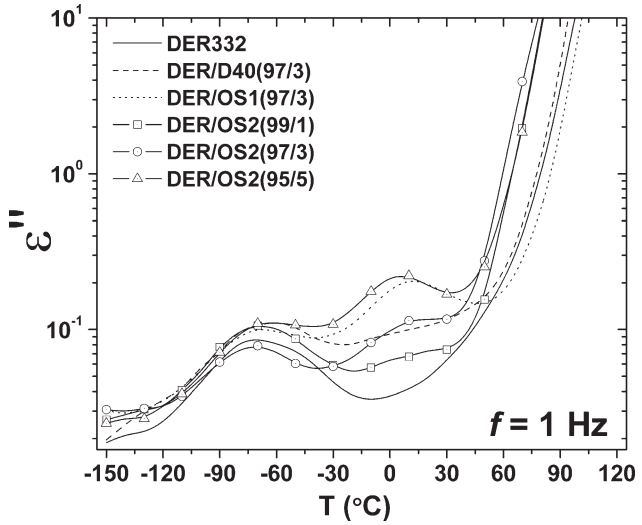

Figure 6 Isochronal (constant frequency) plot of dielectric loss ε" against temperature T at 1 Hz for several compositions indicated on the plot.

are shifted to higher temperatures, as compared with the TSDC thermograms of Figure 4, because of the higher frequency of presentation (1 Hz against 10^{-4}–10^{-2} Hz). We will discuss the results for these two relaxations in relation also to the TSDC plots in Figure 4 and the DMTA plots in Figure 3 later by considering also the corresponding isothermal comparative plots. The steep increase of dielectric loss at higher temperatures approaching T_g reflects dc conductivity, as discussed for sample DER/OS2 (95/5) in Figure 5. We will come back to dc conductivity later.

The corresponding to Figure 6 isochronal plot of real part of dielectric permittivity ε′ against temperature T for the same compositions is shown in Figure 7, however now at the highest frequency of measurements of 1 MHz, to get rid of conductivity effects and focus on dipolar effects. The increase of ε′ with increasing T for each composition is rather trivial, as it reflects the expected for a polymer in the glassy state increase of molecular mobility with increasing temperature, as more and more frozen motions are gradually released. More interesting is the significant increase of ε′ at each temperature for all Ncs as compared with the neat epoxy matrix. An increase of dielectric constant on addition of nanofillers has been observed also in epoxy/alumina nanowires Ncs.[22] The increase of ε′(T) in the Ncs as compared with the neat epoxy matrix in Figure 7 reflects increased mobility in the Ncs and is at the origin of the overall decrease of the storage modulus E' of epoxy resin on addition of the nanofiller presented in Figure 3 and the corresponding increase of the toughness discussed in the section where the DMTA results were presented. In consistency with this interpretation, the sample DER/OS1(97/3), characterized by the lowest E' (T) values in Figure 3, shows the highest ε′(T) values, *i.e.*, the highest mobility in the glassy state in Figure 7. Moreover, comparative isothermal ε′(f) plots at low temperatures (in the glassy state), not shown here, reveal that for the samples with a fixed filler fraction of 3 mass % ε′ increase in the order DER, D40, OS2, OS1, whereas E' (T) in Figure 3 decreases in exactly the same order. Different results have been obtained in other polymer Ncs, such as epoxy/clay Ncs,[43] polycyanurate/clay Ncs,[44] and polyimide/silica Ncs,[45] where rigid nanofillers interact with the matrix, in some cases being covalently attached to the chains, and impose constraints to the motion of the polymeric chains, resulting in a reduction of ε′ in the glassy state. Please note that this represents a common route for preparing materials with low values of ε′ (low-k materials) for microelectronics applications.[45]

The next two figures, Figures 8 and 9, show comparative ε″(f) plots at selected temperatures, −140 and 10°C, respectively, for several compositions, to facilitate discussion on the effects of nanoparticles on the γ and on the β and ω relaxations, respectively.

We recall that the γ relaxation could not be studied neither by DMTA (Fig. 3) nor by TSDC (Fig. 4), being in both cases out of the temperature range of measurements at the low frequencies of these techniques. Owing to this difficulty, data on the γ relaxation in epoxies are rather scarce in literature (compared, for example, with the β relaxation) coming mostly from broadband DRS. Systematic DRS studies in neat DGEBA (typically EPON 828) and mixtures with amines at various stages of

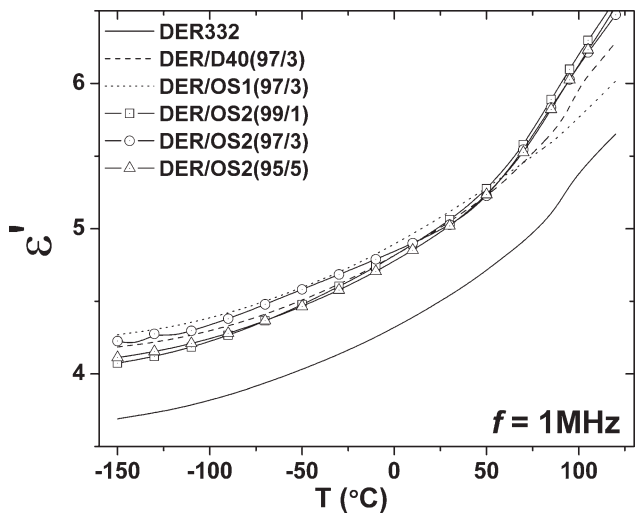

Figure 7 Isochronal (constant frequency) plot of real part of dielectric permittivity ε′ against temperature T at 1 MHz for several compositions indicated on the plot.

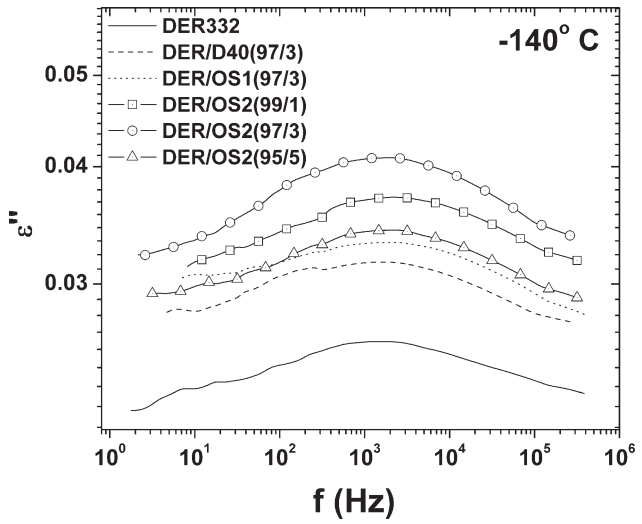

Figure 8 Isothermal $\varepsilon''(f)$ spectra for the compositions indicated on the plot at −140°C to follow effects of the filler on the γ relaxation.

polymerization and network formation (unreacted, partially polymerized, fully polymerized) show that the time scale of the γ relaxation remains practically unchanged, whereas its relaxation strength decreases, becoming so small in fully reacted systems that the relaxation can no more be resolved.[39,40,46,47] These results support the notion that the γ relaxation arises from the motion of localized dipoles of the epoxide end groups. These are consumed during reaction, so that the strength of the relaxation decreases and the process approaches extinction at the final stages of polymerization.[47] Thus, the relatively large strength of the γ relaxation in Figure 8 suggests that the materials under investigation are incompletely polymerized, which appears reasonable in terms of the relatively soft conditions of curing (2 h at 100°C). For comparison, no γ relaxation could be resolved by DRS (in contrast to a clear β relaxation) in epoxy/carbon Ncs prepared from Araldite, diethylenetriamine, and carbon nanoparticles by curing for 3 h at 140°C.[17]

The time scale of the γ relaxation (frequency position of the loss peak in Fig. 8) remains unaffected on addition of filler. This result was confirmed by isothermal plots, similar to those in Figure 8, at several temperatures and by isochronal plots, similar to those in Figure 6 but at higher frequencies. Additional evidence will be provided by analysis of the DRS data in the next section. The magnitude of the relaxation (maximum of loss peak), however, increases in the Ncs, as compared with the neat epoxy, in agreement with the overall increase of $\varepsilon'(T)$ in the glassy state shown in Figure 7. This increase will be quantified by analysis in the next section.

We turn now our attention to Figure 9 and the β relaxation. We recall that this relaxation has been studied also by TSDC (Fig. 4) and by DMTA (Fig. 3 and Table II). Confirmation that it is the same relaxation studied by three different techniques is provided by comparison of the time scale of the relaxations in Figures 3, 4, and 6, which will be quantified later in terms of analysis and the Arrhenius plot in Figure 10. Similar to the γ relaxation mentioned above, the β relaxation has been systematically studied by DRS studies in neat epoxy resin and mixtures with amines at various stages of polymerization and network formation (unreacted, partially polymerized, fully polymerized).[39,40,46,47] A weak β

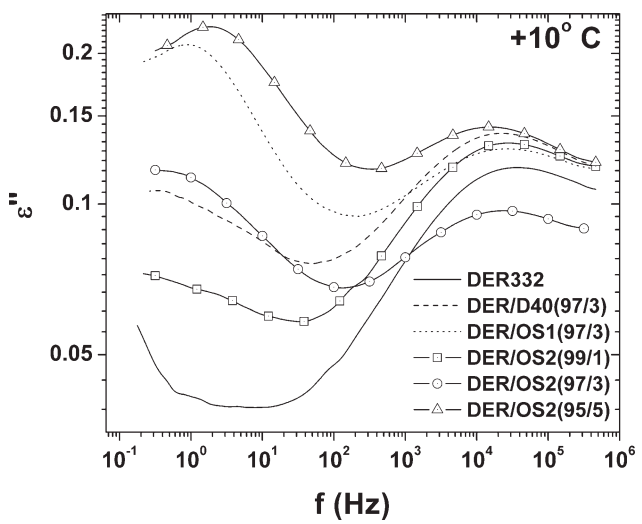

Figure 9 Isothermal $\varepsilon''(f)$ spectra for the compositions indicated on the plot at 10°C to follow effects of the filler on the β and ω relaxations.

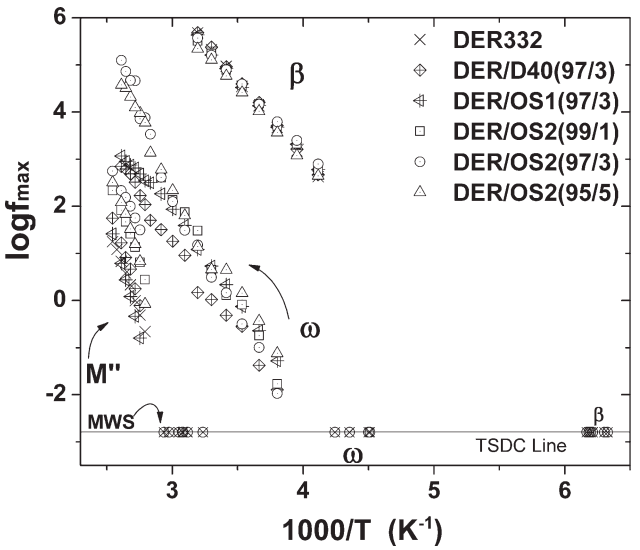

Figure 10 Arrhenius diagram for the materials and the relaxations indicated on the plot. TSDC data have also been included, details in text.

relaxation is present also in neat DGEBA. It becomes faster on addition of amines (unreacted mixtures[47]), whereas in the course of polymerization it becomes slower (although to a smaller extent than the segmental α relaxation) and its magnitude increases. Beiner and Ngai[47] have shown that the β relaxation in the epoxy systems is of the Johari-Goldstein type, *i.e.*, it is the initiator of the α relaxation.

The most pronounced effect of the addition of filler on the β relaxation in Figure 9 is the shift of the loss peak to lower frequencies, *i.e.*, the relaxation is slower in the Ncs as compared with the neat epoxy. Similar results were observed in comparative isothermal plots at lower temperatures (where the β relaxation is shifted to lower frequencies in the central part of our frequency window and can be better studied) and in the isochronal plot of Figure 6. TSDC results in Figure 4 are less conclusive in that respect. The DMTA results at 1 mass % filler in Figure 3 show a similar shift of the relaxation to higher temperatures in the Ncs of about the same extent as in the isochronal DRS plot of Figure 6. It is interesting that, although the frequency of measurements is the same in Figures 3 and 6, the DMTA loss peaks are shifted by about 10°C to higher temperatures as compared with the DRS loss peaks. This is due, at least partly, to the fact that, as typically in DMTA measurements, the loss tangent $\tan\delta = E''/E'$ has been used for the presentation of the data instead of the loss E'', which, due to the drop of E' with increasing temperature, shifts the peak to higher temperatures. It is worth mentioning here that both the position and, in particular, the magnitude of the dielectric β loss peaks in Figures 6 and 9 are affected by the ω relaxation, which shows strong variation with composition. As a result, comparison between the individual Ncs with respect to the magnitude of the β relaxation on the basis of the raw data becomes ambiguous.

A β relaxation with characteristics similar to those in this study has been observed by DRS also in epoxy/alumina nanowires Ncs[22] and in epoxy/carbon Ncs[17] and by DMTA in epoxy/alumina Ncs.[25] The results obtained in the latter study are confirmed by our results, in particular the DMTA results in Figure 3 and Table II, where direct comparison is more straightforward because of the same technique. In both cases an antiplasticization effect of the alumina filler was observed, *i.e.*, a shift of the loss peak to higher temperatures/lower frequencies and a decrease of peak height. Analysis of the data in that work indicated, in agreement with previous work,[41] that the β relaxation in epoxy is double and that the high-temperature part of the relaxation was suppressed on addition of the alumina filler.[25] The two parts of the relaxation have been attributed to local motions at the spatial scale of one epoxy-amine repeat unit (lower temperature part) and to cooperative motions involving at least six units (higher temperature part).[41] The shape of the β loss peak in Figure 3 is consistent with a double character of the relaxation, in agreement also with results of a previous study in epoxy by means of a peak resolving thermal sampling mode of TSDC.[38] Heterogeneity of the network in terms of regions with lower and higher density was considered as responsible for the double character of the β relaxation.[38] On the other hand, using atomic force microscopy Duchet and Pascault[48] showed that epoxy-amine networks can be homogeneous at the nanometric scale. Nevertheless, the TSDC results in Figure 4, in particular the presence of the interfacial MWS peak in all the thermograms, are in favor of a heterogeneous nature of both the neat epoxy and the Ncs under investigation here.

In contrast to the results for the γ and β relaxations presented above, results are less clear for the third secondary relaxation ω. Neither the time scale (position) nor the magnitude of the relaxation change systematically with composition and alumina particle modification in both DRS (Figs. 6 and 9) and TSDC measurements (Fig. 4). The scattering in the magnitude of the relaxation is particularly pronounced. In a previous work on epoxy networks the ω relaxation has been studied in detail by TSDC and attributed to motions of phenyl rings in the looser part of the heterogeneous network,[38] which might be consistent with the large variations from composition to composition. Please note that a relaxation with similar time scale and significant scattering in the magnitude has been observed also by DMTA on the same samples (Fig. 3, tan δ peak at about 30°C).

Analysis of the DRS data

The DRS data at each temperature for each of the three relaxations γ, β, and ω, similar to those shown in Figures 5, 8, and 9, were analyzed by fitting the Havriliak-Negami (HN) model function[17,28]

$$\varepsilon^*(\omega) = \varepsilon_\infty + \frac{\Delta\varepsilon}{(1 + (i\omega\tau)^\alpha)^\beta} \quad (1)$$

to the data. In this equation $\Delta\varepsilon = \varepsilon_s - \varepsilon_\infty$ is the dielectric strength with $\varepsilon_s = \lim_{\omega\tau<<1}(\varepsilon'(\omega))$ and $\varepsilon_\infty = \lim_{\omega\tau>>1}(\varepsilon'(\omega))$, τ the characteristic time scale of the process and ω the angular frequency ($\omega = 2\pi f$) of the applied electric field. Parameters α and β describe the symmetric and asymmetric broadening of the loss peak, where $m = \alpha$ represents the slope on the low frequency side of the dielectric response and $n = \alpha\beta$ the slope on the high frequency side. In the case $\beta = 1$, the HN model function becomes the

Cole-Cole model function. When more than one peaks are present in the $\varepsilon''(f)$ (β and ω relaxations, Fig. 9) a sum of HN terms is used, while the contribution of conductivity (at higher temperatures, overlapping with the ω relaxation, as indicated in Fig. 5) is described by adding in HN eq. (1) the term $K\omega^{-s}$, where K and s are constants.[28]

This kind of analysis provides information on the time scale (τ), the magnitude (relaxation strength, Δε) and the shape (α, β) of each of the relaxations. Analysis showed that the three relaxations are symmetric (β = 1), as often observed for secondary relaxations.[28,44] In what follows, we focus mainly on the time scale of the relaxations, the most significant information extracted from the analysis. This was further analyzed in terms of the Arrhenius diagram by plotting the logarithm of the frequency of maximum dielectric loss, $f_{max} = 1/2\pi\tau$, obtained at each temperature from the HN analysis, against reciprocal temperature (Fig. 10, we note here that due to symmetric shape of the relaxation peaks (β = 1) the characteristic frequency obtained by the HN analysis coincides with the frequency of maximum dielectric loss). In the following, we present and discuss the results obtained by the analysis for the three relaxations γ, β, and ω.

Results for the time scale of the γ relaxation are not included in Figure 10 to expand the reciprocal temperature axis and show results for the other two relaxations in more details. As mentioned in the previous section, the time scale of the γ relaxation does not change with composition (Fig. 8). The temperature dependence of the time scale of the relaxation is well described by the Arrhenius equation[28,44]

$$f_{max} = f_0 \exp\left(\frac{-E_a}{kT}\right) \quad (2)$$

where f_0 is the pre-exponential factor, E_a is the activation energy and k is Boltzmann's constant. The values of the activation parameters, $E_a = 0.30$eV and f_0 in the range of 10^{15} Hz, common to all compositions studied, are in the range of values reported for epoxy networks in the literature (Ref. 47 and references therein). The relaxation strength Δε, obtained by the HN analysis, increases for each composition systematically with increasing temperature. Mean values over the temperature range of measurements for this relaxation are in the range 0.5–0.6, increasing slightly in the Ncs as compared with the neat epoxy network, however by far not as much as it might be suggested by Figure 8. This is often so in polymer Ncs, where an overall increase of the dielectric response is observed, attributed to increased conductivity and conductivity effects[17] and/or increase of the internal electric field.[49] As mentioned above the relaxation is symmetric (shape parameter β = 1). For each composition the shape parameter α decreases with increasing temperature and mean values over the temperature range of measurements are in the range 0.15–0.20 without any systematic variation with composition. The small value of α is consistent with the results shown in Figure 8 where the relaxation extends over several decades, as typically observed for secondary γ relaxations in polymeric materials.[5,44]

Results of the analysis are less unambiguous for the β and ω relaxations, because of overlapping of the two and of the latter with conductivity (Figs. 5, 6, and 9). The temperature dependence of the β relaxation (Fig. 10) is described by the Arrhenius eq. (2). Please note the good agreement with the TSDC data in Figure 10. The TSDC points are determined by the temperature of the TSDC peak (Fig. 4) and the equivalent frequency of TSDC measurements taken as 1.6×10^{-3} Hz, corresponding to a relaxation time of 100 s.[9,29] The shift of the β relaxation to lower frequencies/higher temperatures on addition of the filler (anti-pasticization, Figs. 6 and 9) is not reflected in the activation parameters E_a and f_0 of the Arrhenius eq. (2), which show unsystematic scattering with composition around mean values of 0.60 eV and 10^{15} Hz, respectively. Values in the same range have been reported for various epoxy networks.[17,37,38,47] For each composition the relaxation strength Δε and the shape parameter α show little variation with temperature and no systematic variation with composition being in the range 0.7–1.0 and around 0.35, respectively.

Results for the ω relaxation in the literature are scarce.[37,38] The temperature dependence of the time scale of the relaxation is described by the Arrhenius eq. (2), with values of E_a in the range 0.70–1.00 eV. Rather good agreement between DRS and TSDC data is observed (Fig. 10). For each composition the shape parameter α shows little variation with temperature, whereas the relaxation strength Δε increases significantly with increasing temperature above about 50°C. The relaxation is stronger and more narrow than the other two (Δε and α in the range 1.0–1.3 and 0.45–0.50, respectively).

Conductivity and conductivity effects were analyzed in terms of ac conductivity σ_{ac} and of electric modulus M. σ_{ac} was calculated from the measured dielectric loss (imaginary part of dielectric permittivity) ε'' by means of[28,50]

$$\sigma_{ac}(f) = \varepsilon''(f)\omega\varepsilon_0 \quad (3)$$

where ε_o is the permittivity of free space.

Figure 11 shows comparative plots of $\sigma_{ac}(f)$ for the six compositions studied by dielectric techniques at a relatively high temperature (120°C), where all

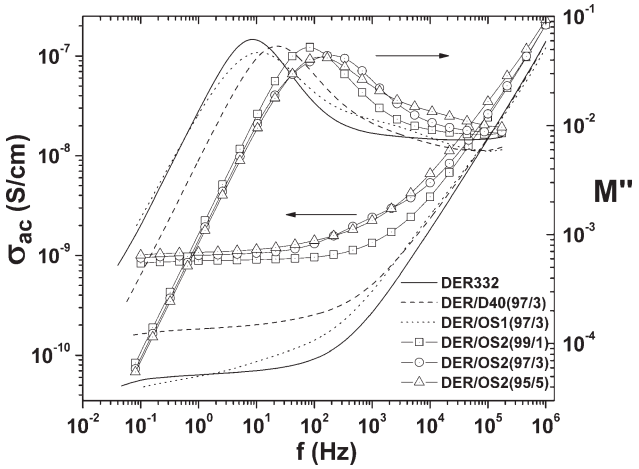

Figure 11 Comparative plot of ac conductivity and of imaginary part of electric modulus M'' against frequency f at 120°C for the samples indicated on the plot.

samples are well above their T_g (Table II). We observe for each composition the well-known behavior of change from frequency independence at low frequencies (plateau, dc conductivity) to strong frequency dependence at higher frequencies (ac conductivity).[50] The different values of dc conductivity for different compositions should be related with the type of modifier used (addition of charge carriers) rather than with morphology and polymer dynamics. We observe in Figure 11, more clearly for some compositions, a structure (shoulder) in $\sigma_{ac}(f)$, *e.g.*, at about 1 kHz for sample DER/OS2 (97/3). This shoulder should be related with interfacial polarization[51] and its investigation may provide information on morphology. To facilitate discussion on that we have included in Figure 11 plots of the imaginary part of electric modulus M'' at the same temperature of 120°C. The complex electric modulus M^* is defined by[52]

$$M^*(f) = \frac{1}{\varepsilon^*(f)} = M'(f) + iM''(f) \quad (4)$$

The electric modulus formalism has proved effective in analyzing ionic conductivity and interfacial effects in amorphous materials.[51,52] $M''(f)$ shows a peak in the frequency range of change from dc to ac conductivity (conductivity relaxation) and, similar to $\varepsilon''(f)$, additional peaks corresponding to dipolar and interfacial relaxations.[51] This is evident for DER/OS2 (97/3) sample, where a double peak is observed, the higher frequency component corresponding to the shoulder in the $\sigma_{ac}(f)$ plot. To make that more clear and to stress the methodological aspect, we compare in Figure 12 the frequency dependence of various relaxation functions, including $\sigma_{ac}(f)$ and $M''(f)$, for DER/OS2 (97/3) sample of Figure 11, now at the more convenient temperature of 90°C. We observe that the higher frequency component in M'' corresponds, in addition to the shoulder in $\sigma_{ac}(f)$ discussed above, also to weaker structures in $\varepsilon''(f)$ and in tan $\delta(f)$ [shifted to lower frequencies as a result of the transformation in eq. (4)[51]]. Each of these structures can be used to study interfacial polarization/relaxation, modulus being often more convenient for that.

We turn back to Figure 10 in relation to interfacial polarization. It is out of the scope of this article to analyze in detail interfacial effects within the different formalisms. For that reason we show in Figure 10 data for the frequency of maximum of the M'' dispersion corresponding to conductivity relaxation and interfacial polarization (Figs. 11 and 12) without further analysis. It is evident that the data for M'' correspond well to the TSDC data for the MWS interfacial polarization, which provides further support for the interpretation of the M'' data. The temperature dependence of these data seems to follow the Vogel-Tammann-Fulcher (VTF) behavior, characteristic for the glass transition,[53] rather than the Arrhenius behavior. This would suggest that the conductivity mechanism at the origin of the interfacial polarization/relaxation is governed by the motion of the polymeric chains. For a proper analysis of the temperature dependence of the M'' data in Figure 10 and discussion of the results in terms of morphology, we should first analyze the frequency dependence of the M^* data (similar to those shown in Fig. 11) by using proper model functions. It would be interesting to further follow this point in future work.

CONCLUSIONS

DMTA and two complementary dielectric techniques, broadband DRS and TSDC, were employed to

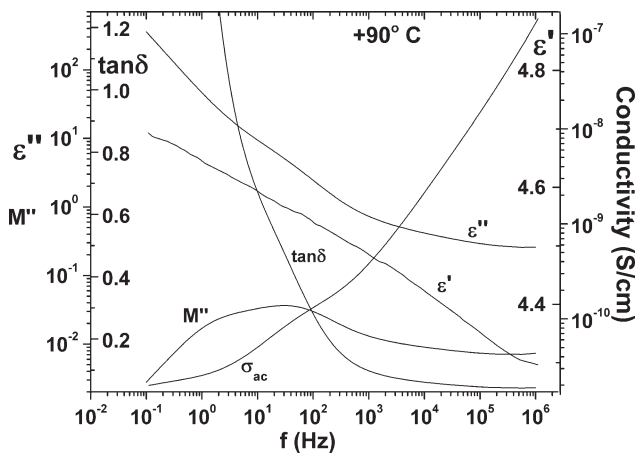

Figure 12 Comparative plot of various dielectric functions, ε', ε'', tan δ, M'', ac conductivity, against frequency f for the sample DER/OS2(97/3) at 90°C.

study in details effects of nanoparticles on polymer dynamics in epoxy/alumina nanocomposites of various compositions prepared by dispersing modified and nonmodified boehmite nanoparticles in DGEBA and using diethylenetriamine as curing agent. Viscosity measurements in the nanodispersions before polymerization provided information on the quality of the dispersion of particles and on morphology, which was correlated with morphology and dynamics of the cured samples. SEM on fractured samples was used for morphological characterization of the cured samples.

Five relaxations were observed and analyzed by the combination of the three techniques: the secondary γ, β, and ω relaxations in the glassy state, the segmental α relaxation, associated with the glass transition, and the interfacial MWS relaxation, associated with the heterogeneous structure of the samples. Effects of the type (modification) and of the amount of filler on the time scale, the magnitude and the shape of the relaxations were studied, where possible quantified, and discussed in relation to previous work on similar systems. Next to complementarity, the results revealed interesting correlations between the various techniques, in particular a correlation between viscosity (of the nanodispersions), storage modulus, glass transition temperature, real part of dielectric permittivity, and ductility. This correlation provides additional support for the notion that rheological measurements in the nanodispersions before polymerization are a powerful tool for optimizing processing conditions.[17,54] In addition, the correlation between increase of the real part of dielectric permittivity $\varepsilon'(f)$ (*i.e.*, increase of molecular mobility), decrease of the storage modulus and increase of ductility on addition of nanoparticles and depending on the type of modification, may provide a basis for using dielectric measurements, easily available over wide ranges of frequency and temperature, to predict mechanical properties. Finally, the investigation of conductivity and interfacial polarization/relaxation provides information on morphology, as motion and trapping/release of ions probe local morphology. This point should be further followed in future work by proper analysis of the corresponding dielectric data within different formalisms.

The authors thank Dr. A. Malyschew, Sasol (Germany) for kindly providing the boehmite alumina nanofillers.

References

1. Alexandre, M.; Dubois, P. Mater Sci Eng 2000, 28, 1.
2. Sanchez, C; Soler-Illia, C. J de A. A.; Ribot, F.; Lalot, T.; Mayer, C. R.; Cabuil, W. Chem Mater 2001, 13, 3061.
3. Ray, S. S.; Okamoto, M. Prog Polym Sci 2003, 28, 1539.
4. Coleman, J. N.; Cadek, M.; Ryan, K. P.; Fonseca, A.; Nagy, J. B.; Blau, W. J.; Ferreira, M. S. Polymer 2006, 47, 8556.
5. Kourkoutsaki, T.; Logakis, E.; Kroutilova, I.; Matejka, L.; Nedbal, J.; Pissis, P. J Appl Polym Sci 2009, 113, 2569.
6. He, F.; Wang, L. M.; Richert, R. Phys Rev B 2005, 71, 144205.
7. Scheidler, P.; Kob, W.; Binder, K. J Phys Chem B 2004, 108, 6673.
8. Alcoutlabi, M.; McKenna, G. B. J Phys Condens Mater 2005, 17, R461.
9. Fragiadakis, D.; Pissis, P.; Bokobza, L. Polymer 2005, 46, 6001.
10. Fragiadakis, D.; Pissis, P. J Non-Crystal Solids 2007, 353, 4344.
11. Bershtein, V. A.; Egorova, L. M.; Yakushev, P. N.; Pissis, P.; Sysel, P.; Brozova, L. J Polym Sci Part B Polym Phys 2002, 40, 1056.
12. Goertzen, W. K.; Kessler, M. R. Compos A 2008, 39, 761.
13. Becker, O.; Simon, G. P. Adv Polym Sci 2005, 179, 29.
14. Sun, Y.; Zhang, Z.; Moon, K.-S.; Wong, C. P. J Polym Sci Part B Polym Phys 2004, 42, 3849.
15. Miyagawa, H.; Rich, M. J.; Drzal, L. T. J Polym Sci Part B Polym Phys 2004, 42, 4384.
16. Lu, H.; Nutt, S. Macromolecules 2003, 36, 4010.
17. Kotsilkova, R.; Fragiadakis, D.; Pissis, P. J Polym Sci Part B Polym Phys 2005, 43, 522.
18. Ash, B. J.; Siegel, R. W.; Schadler, R. S. J Polym Sci Part B Polym Phys 2004, 42, 4371.
19. Ash, B. J.; Siegel, R. W.; Schadler, R. S. Macromolecules 2004, 37, 1358.
20. Long, D.; Lequeux, F.; Eur Phys J E 2001, 4, 371.
21. Narayanan, R. A.; Thiyagarajan, P.; Lewis, S.; Bansal, A.; Schadler, L. S.; Lurio, L. B. Phys Rev Lett 2006, 97, 075505.
22. Wan, T.-W.; Yu, D.-M.; Huang, L.-B.; Xie, Y.-C.; Guo, X.-S.; Zhang, J. Macromol Chem Phys 2008, 209, 1056.
23. Kim, D.; Lee, J. S.; Barry, C. M. F.; Mead, J. L. Polym Eng Sci 2007, 47, 2049.
24. Kuo, M. C.; Tsai, M. C.; Huang, J. C.; Chen, M. Mater Chem Phys 2005, 90, 185.
25. Vassileva, E.; Friedrich, K. J Appl Polym Sci 2003, 89, 3774.
26. Gatos, K. G.; Martinez Alcazar, J. C.; Psarras, G. C.; Thomann, R.; Karger-Kocsis, J. Compos Sci Technol 2007, 67, 157.
27. Rittigstein, P.; Torkelson, J. M. J Polym Sci Part B Polym Phys 2006, 44, 2935.
28. Kremer, F.; Schoenhals, A., Eds. Broadband Dielectric Spectroscopy; Springer: Berlin, 2002.
29. Van Turnhout, J. In Electrets, Sessler, G. M., Ed.; Springer: Berlin, 1980, p 81.
30. Sangermano, M.; Deorsola, F.; Fabiani, D.; Montanari, G.; Rizza, G. J Appl Polym Sci 2010, 114, 2541.
31. Tanaka, T. In Dielectric Polymer Nanocomposites; Nelson, J. K., Ed.; Springer: Berlin, 2010, Chapter 8.
32. Kozako, M.; Ohki, Y.; Kohtoh, M.; Okabe, S.; Tanaka, T. IEE J Trans Fund Mater 2007, 126, 1121.
33. Zheng, Y.-P.; Zhang, J.-X.; Li, Q.; Chen, W.; Zhang, X. Polym Plast Technol Eng 2009, 48, 384.
34. Khumalo, V. M.; Karger-Kocsis, J.; Thomann, R. Exp Polym Lett 2010, 4, 264.
35. Streller, R. C.; Thomann, R.; Torno, O.; Muehlhaupt, R. Macromol Mater Eng 2009, 294, 380.
36. Brostow, W.; Datashvill, T.; Kao, D.; Too, J. Polym Compos 2010, 31, 417.
37. Delides, C. G.; Vatalis, A. S.; Pissis, P.; Pethrick, R. A. J. Macromol Sci Phys 1993, B32, 261.
38. Maggana, C.; Pissis, P. J.; Macromol Sci Phys 1993, B36, 749.
39. Mangion, M. B. M.; Johari, G. P. J Polym Sci Part B Polym Phys 1990, 28, 71.
40. Mijovic, J; Zhang, H. Macromolecules 2003, 36, 1279.
41. Heux, L.; Halary, J. L.; Laupretre, F.; Monnerie, L. Polymer 1997, 38, 1767.

42. Wübbenhorst, M.; van Turnhout, J. J Non-Cryst Solids 2002, 305, 40.
43. Kanapitas, A.; Pissis, P.; Kotsilkova, R. J Non-Cryst Solids 2002, 305, 204.
44. Maroulas, P.; Kripotou, S.; Pissis, P.; Fainleib, A.; Bei, I.; Bershtein, V.; Gomza, Y. J Compos Mater 43:943 2009.
45. Kramarenko, V. Y.; Shantalii, T. A.; Karpova, I. L.; Dragan, K. S.; Privalko, E. G.; Privalko, V. P.; Fragiadakis, D.; Pissis, P. Polym Adv Technol 2004, 15, 144.
46. Wasylyshyn, D. A.; Johari, G. P. J Chem Phys 1996, 104, 5683.
47. Beiner, M.; Ngai, K. L. Macromolecules 2005, 38, 7033.
48. Duchet, J.; Pascault, J. P. J Polym Sci Part B Polym Phys 2003, 41, 2422.
49. Page, K. A.; Adachi, K. Polymer 2006, 47, 6406.
50. Kyritsis, A.; Pissis, P.; Grammatikakis, J. J Polym Sci Part B Polym Phys 1995, 33, 1737.
51. Georgoussis, G.; Kanapitsas, A.; Pissis, P.; Savelyev, Yu. V.; Veselov, V. Ya.; Privalko, E. G. Eur Polym Mater 2000, 36, 1113.
52. Macedo, P. B.; Moynihan, C. T.; Bose, R. Phys Chem Glass 1972, 13, 171.
53. Donth, E. The Glass Transition: Relaxation Dynamics in Liquids and Disordered Materials; Springer: Berlin, 2001.
54. Kotsilkova, R., Ed. Thermoset Nanocomposites for Engineering Applications; Rapra: Shawbury, 2007.